External Inertia Emulation Controller for Grid-following Power Converter

Ngoc Bao Lai, *Student, IEEE*, Andres Tarrasó, *Student, IEEE*, Gregory N. Baltas, *Student, IEEE*, Leonardo Marin, *Student, IEEE*, and Pedro Rodriguez, *Fellow, IEEE*

***Abstract*—The advent of renewable energy has posed difficulties in the operation of power systems whose net inertia is becoming critically low. To face such challenges, grid-forming power has been one of the potential solutions pursued by the industry and research community. Though promising, grid-forming power converters are still immature for mass deployment in power systems. In the meanwhile, an enormous amount of grid-following power converters has been underexploited when it comes to grid-supporting functionalities. Therefore, this paper proposes an external inertia emulation controller (eIEC) for grid-following power converter to provide frequency support to the grid. For the purpose of minimizing installation efforts and resources, the controller is designed in such a way that it can be implemented in an external controller communicating with the grid-following power converter via an industrial communication link. This paper also investigates the effect of communication delay on the stability performance of the proposed controller. In addition to the detailed analysis, hardware-in-the-loop experiments are also carried out to validate the proposed eIEC.**

***Index Terms*—Inertia emulation, Grid-following power converter, networked control, low inertia systems, frequency support.**

I. Introduction

In an effort towards carbon neutrality, the installation of renewable energy has increased significantly in the last decade. According to the latest estimates, the worldwide capacity addition of renewables has risen from 54.5 GW in 2010 to 198 GW in 2020 [1]. Despite the positive environmental impact, the large-scale integration of renewables, which connects with the grid mainly via grid-following power converters, threatens the operation of power systems. Particularly, since the grid-following power converters do not possess inertial behavior, the net inertia of power systems has been continuously reducing. This reduction in system inertia results in a higher rate of change of frequency (RoCoF) and maximum frequency deviation, which can lead to frequency instability, load-shedding or even blackout [2]. Thus, improving frequency stability for power systems, especially for those with high-level of renewable penetration, has become an important issue [3]. Indeed, fast frequency reserve has been introduced as a service in recent grid codes to cope with low-inertia situations [4].

The most conventional and widely adopted control approach to mitigate the adverse impact of large-scale integration of renewables on frequency stability is to emulate inertia by using power converters [5], [6]. That is, by modifying its control part, the power converters can provide inertia response to a grid frequency deviation. Consequently, the net inertia of the system can be increased to reduce both the RoCoF value and the maximum frequency deviation. Existing inertia emulation approaches are either direct or indirect. Direct methods aim to increase the system inertia by injecting active power inversely proportional to the derivative of frequency deviation, modifying exclusively the inertia constant of the power system. Being virtually implemented in a controller, the value of virtual inertia can be modified arbitrarily in a given range to meet the desired performance. A controller that takes advantage of the dc-link capacitor for emulating inertia is presented in [7]. In this study, the injected power is set to be directly proportional to the derivative of frequency which is obtained from a phase-locked loop (PLL). To avoid the direct implementation of the derivative operator that might lead to instability, a washout filter is often employed [8]. Though direct inertia emulation is simple and theoretically sound, the high level of susceptibility to measurement noises hinders its practical deployment.

On the other hand, the indirect inertia emulation methods emulate partially or fully the operation of a synchronous machine (SM) also referred to as virtual synchronous machine (VSM) [9]. With these indirect methods, the power converter can operate as a SM to provide frequency support and other grid-friendly functionalities without directly modifying the inertia constant of the power system. The power converters equipped with this control group is recently identified as grid-forming power converters [10]. Due to its versatility and practicality, grid-forming power converter has received increasing attention from the industry and research community.

Manuscript received April 22, 2021; revised July 13, 2021; accepted August 19, 2021. Paper 2021-IACC-0336.R1, presented at the 2020 Energy Conversion Congress and Exposition, Detroit, MI USA, Oct. 11–Oct. 15, and approved for publication in the IEEE TRANSACTIONS ON INDUSTRY APPLICATIONS by the Industrial Automation and Control Committee of the IEEE Industry Applications Society. This work was supported by the European Commission under Project FLEXITRANSTORE-H2020-LCE-2016-2017-SGS-774407. *(Corresponding author: Ngoc Bao Lai.)*

Ngoc Bao Lai, Gregory N. Baltas, and Pedro Rodriguez are with the Intelligent Clean Energy System (ICES) unit, Luxembourg Institute of Science and Technology (LIST), Esch-Sur-Alzette, L-4362, Luxembourg (e-mail: laingocbao@gmail.com, gregory.baltas@list.lu, and pedro.rodriguez@list.lu).

Andres Tarrasó and Leonardo Marin are with the research center on Renewable Electrical Energy Systems (SEER), Universitat Politècnica de Catalunya (UPC), 08034, Barcelona, Spain (email: andres.tarraso@upc.edu and lvmarin@uloyola.es).

Common implementations of grid-forming power converters include voltage and current cascaded controller [11], synchronverter [12], synchronous power controller (SPC) [13], and more recently virtual oscillator [14]. Due to its simplicity and robustness, the SPC implementation is preferable. Because grid-forming power converters can provide inertia response similar to a SM, it contributes to improving frequency stability of power systems as demonstrated in recent works [15], [16].

A number of extended studies on the aforementioned inertia implementation approaches for grid-tied power converters have been recently conducted. Notably, [17] investigated the behavior of commercial inverters in the event of grid frequency deviations. Evidently, frequency-watt droop function, which resembles primary frequency regulation, can contribute positively to arresting frequency excursions. Demonstrations of the direct inertia emulation approach have also been reported. Authors in [18] [19] proposed a simple controller, that consists of a derivative block connected in series with a virtual inertia gain, for generating damping power. As an enhancement, a lead-lag compensator is introduced after the derivative block in [20] to deal effectively with measurement noises. Being more straightforward and grid friendly, virtual inertia implementation based on VSM is widely adopted. Remarkably, [21] validates the effectiveness of VSM in providing grid frequency support for the two-area system. A simplified version of VSM for grid-following converters is also proposed in [22]. Usually, VSM consists of an electromechanical part and an electromagnetic part. The former often implements a swing equation to equip the converter with electromechanical dynamics. Likewise, the latter includes virtual admittance to characterize the electromagnetic behavior of the power converter.

Nevertheless, the actual implementation of all the above methods requires a modification of the control firmware of the power converters. Considering the enormous amount of already deployed converters, which are mainly programmed to work as grid followers, the requirement of firmware modification is deemed impractical and costly due to the additional development effort needed for testing and certifications. As an alternative, inertia emulation algorithms might be implemented on an external controller, which communicates with the power converter via a Fieldbus communication link. This is possibly due to a slower frequency response range i.e. between 1 and 10 seconds [23], which is not so demanding in terms of control bandwidth. Towards that end, an earlier research attempt in [24] shows interesting results yet the design and analysis of the controller are still limited.

Motivated by the above rationale, this paper proposes an external inertia emulation controller (eIEC) interfacing with the power converter through a communication link. This implementation provides the ability for plug-and-play operation meaning that the proposed eIEC can enable any grid-following power converter to provide inertia emulation functionality without costly and time-consuming modifications of the internal firmware of the power converter. Moreover, being independent of the power converter system, the eIEC can be standardized to meet grid code requirements, and allow receiving input signals from the transmission system operator (TSO) for altering parameters setting as required in several grid codes [6]. Concretely, this paper analyzes the influence of communication delays caused by such an external implementation on the eIEC performance. Finally, simulations and hardware-in-the-loop (HIL) experiments are carried out for validation purposes.

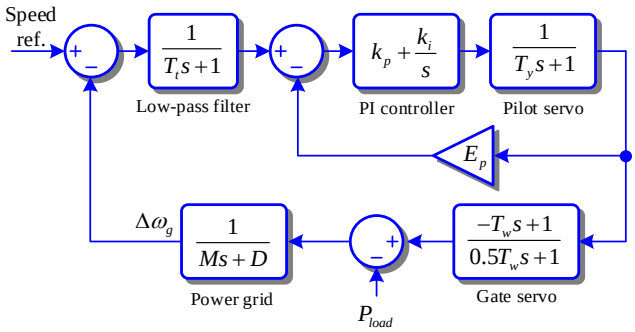

Fig. 1. Equivalent model for Nordic power system.

TABLE I
PARAMETERS OF NORDIC SYSTEM

Symbol	Quantity	Values
T_t	Filter time constant	0.5 s
k_p	Proportional gain	2 pu
k_i	Integral gain	0.49 s^{-1}
E_p	Droop coefficient	0.05 pu
T_y	Servo time constant	0.2 s
T_w	Water time constant	0.5 s
M	Inertia time constant	9.8 s
D	Frequency dependent load	0.9 pu
a_0	Coefficient	0.02265
b_0	Coefficient	0.4531
b_1	Coefficient	0.9937
	Frequency deviation for load shielding	1.5 Hz
	RoCoF for load shielding	0.18 Hz/s

II. SYSTEM MODELING

For the proper design and tuning of the controller, this section presents a brief overview of the grid model typically used for studying frequency regulation, and the model for a conventional grid-following power converter. To facilitate the analysis, the models are linearized and in the continuous-time domain.

A. Grid Model for Frequency Stability Analysis

Conventionally, frequency stability studies are based on a one-area system [25], [26]. In this paper, the model of the Nordic system is considered mainly for two reasons: the high penetration of renewables and the recently observed frequency instability issues [2]. Fig. 1 shows the block diagram of the equivalent model for the Nordic system whose parameters are summarized in Table I [27]. Since the focus of this work is to study the performance of the proposed controller, rather than tuning the PI controller, the low-pass filter, the PI controller, and the servo models are simplified by using the balanced truncation method resulting in a reduced model as in Fig. 2. Such simplification is beneficial for real-time implementation. From Fig. 2, the transfer function of the grid can be derived as

This article has been accepted for publication in IEEE Transactions on Industry Applications. This is the author's version which has not been fully edited and content may change prior to final publication. Citation information: DOI 10.1109/TIA.2021.3108350

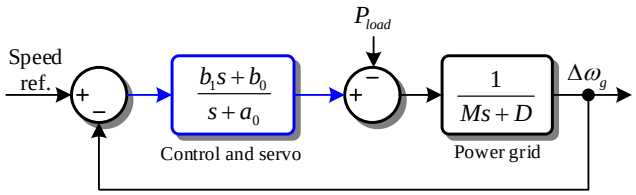

Fig. 2. Reduced model of Nordic power system.

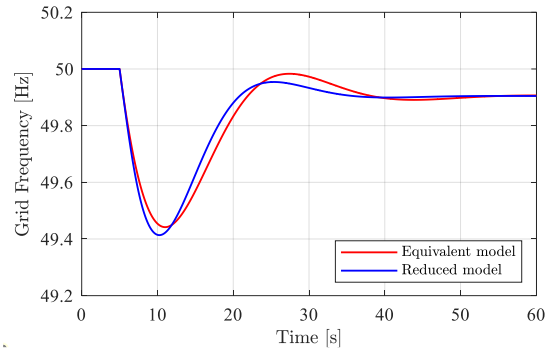

Fig. 3. Response of equivalent and reduced model for Nordic power system.

$$G_{grid}(s)=\frac{\Delta\omega_g(s)}{P_{load}(s)}=\frac{s+a_0}{2Ms^2+(D+b_1+Ma_0)s+b_0+Da_0}. \quad (1)$$

This reduced model will be used not only for tuning the proposed controller but also for hardware-in-the-loop validation. Fig. 3 shows a step response to a load event of the equivalent and reduced model. It is evident that the reduced model is able to capture the dynamics of the Nordic system. Indeed, the frequency dynamics of the reduced model closely match that of the equivalent model, in particular, the during inertia response period.

B. *Model of a Grid-following Power Converter*

To derive the model of a grid-following power converter, without loss of generality, a typical grid-following power converter, which is interfaced with the grid via an LCL-filter, is considered in Fig. 4. The strength of the grid is determined by the equivalent resistance of R_g and inductance L_g. The control part of the power converter consists of a power controller and a current controller, whose main objective is to track the power references P_{ref} and Q_{ref}. Moreover, the grid phase angle is estimated by a phase-locked loop (PLL) implemented on the synchronous reference frame. The closed-loop transfer function of the power converter might be generally defined as $G_{PC}(s)$. Consequently, the complete model including the grid and the power converter is be presented as in Fig. 5.

III. External Inertia Emulation Controller

This section (a) reviews the commonly used communication protocols for grid-connected power converters and their real-time characteristics, (b) presents the proposed eIEC, provides a detailed analysis on the influence of communication delay on the controller performance. The overall block diagram of the

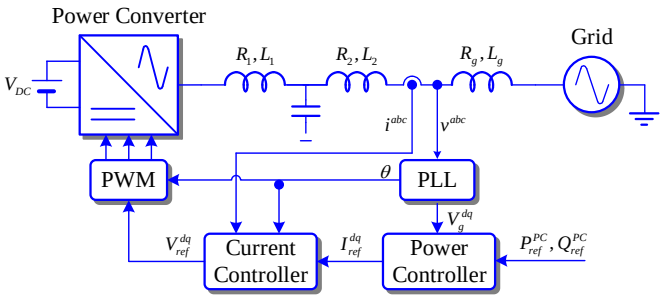

Fig. 4 Configuration and control of a typical grid-following power converter.

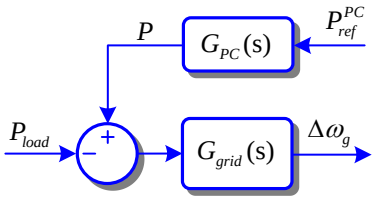

Fig. 5. Grid model with power converter integrated.

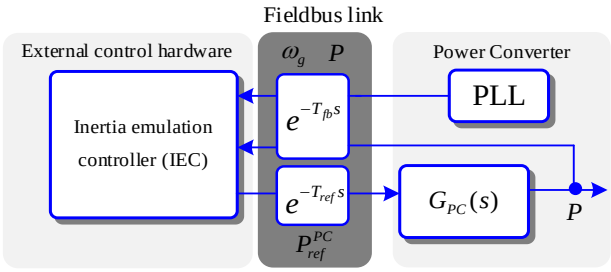

Fig. 6. Overall block diagram of the proposed control scheme.

proposed control scheme is illustrated Fig. 6 where the eIEC provides active power reference to the power converter and receive injected power and grid frequency as feedback signals.

A. *Fieldbus Communications for Power Converter*

Fieldbus defines a family of industrial communication networks for real-time control adopted by the majority of power conversion systems [28]. Due to its robustness, Fieldbus is often used for exchanging operational and control information between power converters and external equipment. For instance, wireless ethernet is employed for controlling submodules for modular multilevel converter [29]. For grid-connected power converters, the most commonly used protocols include controller area network (CAN) bus, Modbus, and EtherCAT [30], [31]. Among these protocols, the EtherCAT has the lowest communication latency, whereas Modbus, especially that based on transmission control protocol (Modbus TCP), often suffers from higher latency and delay. Even though it depends on the network condition and topology, the turnaround time for EtherCAT, CAN, Modbus are often in a range of a few to dozens of milliseconds. As the activation time required for inertia response is from half to even one second [32], clearly, it is possible to implement the eIEC deployed on external control hardware that communicates with the power converter through one of the aforementioned communication interfaces.

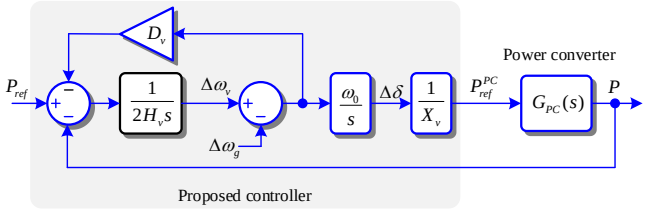

Fig. 7. Proposed external inertia emulation controller (eIEC).

B. *Inertia Emulation Controller*

Fig. 7 shows the proposed eIEC which resembles a synchronous machine. Indeed, the electromechanical interaction of the proposed eIEC is characterized by virtual inertia constant H_v, which can be expressed as

$$G_1(s) = \frac{1}{2H_v s}. \tag{2}$$

To achieve synchronization with the grid, the virtual angle frequency is compared with measured grid frequency, and then the frequency deviation is integrated to obtain the angle deviation as

$$\frac{\Delta\delta(s)}{\Delta\omega_v(s) - \Delta\omega_g(s)} = \frac{\omega_0}{s} \tag{3}$$

where ω_0 denotes the nominal angular frequency.

Since the majority of grid-following power converters receive references in terms of active and reactive power, it is necessary to convert the angle deviation into power references. By using the conventional power-follow equation, the angle deviation can be transformed into active power as

$$P = \frac{V_{inv}}{R^2 + X^2}\left[R_V\left(V_{inv} - V_g\cos(\Delta\delta)\right) + X_{inv}V_g\sin(\Delta\delta)\right] \tag{4}$$

where V_{inv} and V_g are the magnitudes of inverter output voltage and grid voltage, respectively, and R_v and L_v are the virtual resistance and inductance, respectively. Assuming $R_v = 0$, $\sin(\Delta\delta) \approx \Delta\delta$, and $V_{inv} \approx V_g \approx 1$, (4) can be simplified as

$$P_{ref}^2 = \frac{1}{X_v}\Delta\delta. \tag{5}$$

Equations (3), (5), and $G_{PC}(s)$ can be concisely expressed in terms of a transfer function as

$$G_2(s) = \frac{P_{ref}^2(s)}{\Delta\delta(s)} = \frac{\omega_0}{X_v s}G_{pc}(s). \tag{6}$$

The damping coefficient D_v is employed to adjust the damping ratio of the closed-loop system. The higher the value of D_v, the more damped the closed-loop system. However, high value of D_v might result in a slow transient response of the system.

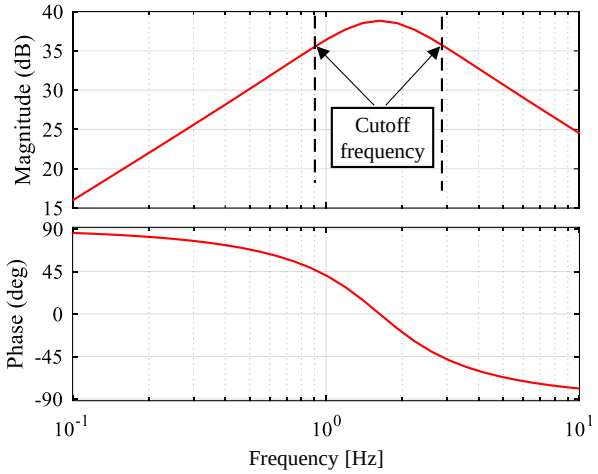

Fig. 8. Frequency response of the eIEC to grid frequency according to (8).

Considering that the power control loop of a grid-following power converter is relatively fast (20-50 ms) compared to the eIEC, it is reasonable to assume $G_{PC}(s) = 1$. Consequently, the can be derived as

$$\frac{P(s)}{P_{ref}(s)} = \frac{\omega_0}{2H_v X_v s^2 + D_v X_v s + \omega_0} \tag{7}$$

$$\frac{P(s)}{\Delta\omega_g(s)} = \frac{D_v X_v s + \omega_0}{2H_v X_v s^2 + D_v X_v s + \omega_0} \tag{8}$$

Note that (7) and (8) take the form of a second-order system with the natural frequency,

$$\omega_n = \sqrt{\frac{\omega_0}{2H_v X_v}}. \tag{9}$$

Generally, the virtual inertia is predetermined by the system operator or the grid codes. Therefore, the damping coefficient D_v might be calculated from the desired damping ratio ζ as follows:

$$D_v = \zeta H_v\sqrt{\frac{8\omega_0}{H_v X_v}}. \tag{10}$$

From (8), the frequency response of the eIEC with regards to grid frequency event can be obtained as in Fig. 8, where the black dashed lines denote lower and upper cutoff frequencies around 1 and 3 Hz. Such cutoff frequency indicates that the eIEC has low sensitivity to high-frequency noises, which are usually present in the frequency measurements due to switching. This property makes the eIEC more preferable in terms of practical implementation than those based on frequency derivatives.

C. *Influence of Communication Delay*

It is obvious from Fig. 6 that the communications will create an unavoidable delay in the control loop that might lead to performance degradation or even instability. Therefore, it is necessary to analyze the impact of the communication delays

on the performance of the eIEC and the grid stability.

The delay, which is introduced by communicating active power reference P_{ref} and the feedback signals ω_g and P, might be presented as

$$T_d = T_{ref} + T_{fb} \tag{11}$$

where T_{ref} is the time needed for P_{ref} to arrive at the power converter and T_{fb} is the communication delay for the feedback signals. For the sake of simplicity, communication delay might be linearized by using first-order Padé approximation as

$$G_d(s) = \frac{2 - 1.5T_d s}{2 + 1.5T_{d\,s}}. \tag{12}$$

Considering the communication delay, the control block diagram depicted in Fig. 7 might be modified as in Fig. 9. Accordingly, equation (6) is redefined as

$$G_{2d}(s) = G_2(s)G_d(s). \tag{13}$$

From Fig. 5, (1), (2), and (13), the transfer function that aggregates the power converter, the eIEC, and the grid can be derived as

$$\frac{P(s)}{\omega_g(s)} = \frac{(D_v G_{grid} + G_{2d} G_{grid})G_1 + G_{grid}}{(D_v + G_{2d})G_1 + G_{2d} G_{grid} + 1}. \tag{14}$$

where the Laplace operator s has been omitted in (14) for brevity. Equation (14) presents a fifth-order system whose dynamic characteristics can be conveniently studied by using root locus and frequency response techniques.

To illustrate, for chosen values of virtual inertia of $H_v = 5\,s$ and virtual impedance of $X_v = 0.3\,pu$, the virtual damping corresponding to $\zeta = 0.707$ can be calculated from (10) as $D_v = 145$. From (14), a root locus with different values of T_{comm}, D_v, and X_v can be obtained as in Fig. 10 in which the arrows indicate changes of closed-loop poles with respect to the increment of selected parameter. It can be observed that as the communication delay increases, the oscillatory pole moves toward the imaginary axis indicating the decline of damping ratio and stability margin. Indeed, the system is unstable as T_{comm} reaches 100 *ms*. To improve the system stability, there are two parameters in the proposed eIEC that can be tuned: the virtual impedance X_v and the damping coefficient D_v. It is obvious from Fig. 10 that the X_v is inversely proportional to the power reference produced by eIEC. Therefore, by decreasing X_v, it is possible to reduce the net gain of eIEC.

Evidently, as shown in Fig. 10, the higher the value of X_v the higher damping ratio. an increase of X_v reduces the magnitude of the inertia response produced by the eIEC. Unless necessary, it is suggested that X_v should not be modified. On the other hand, D_v can also be tuned to achieve better stability.

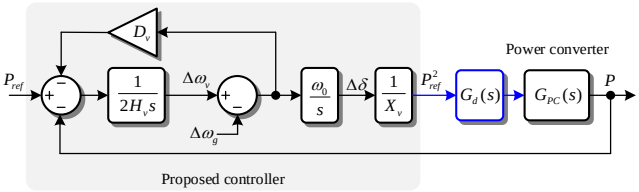

Fig. 9. Closed-loop system with communication delay.

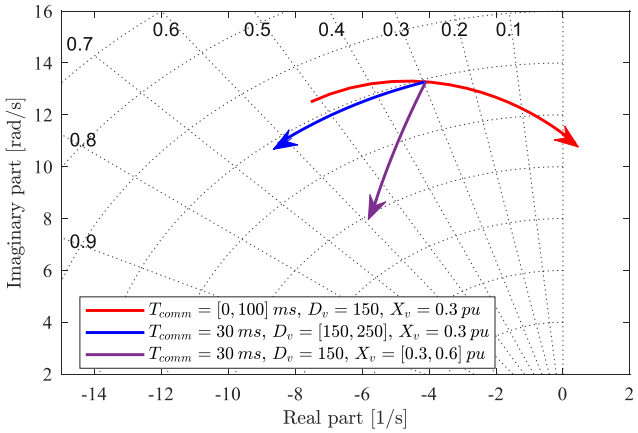

Fig. 10. Root locus of (14) with different values of T_{comm}, D_v, and X_v.

As shown in Fig. 10, the damping ratio can be improved from around 0.3 to 0.6 by increasing D_v from 150 to 250. Because it does not act directly on the output of eIEC, adjusting D_v is preferable for enhancing the system stability.

In addition to stability, it is important to access the performance of the eIEC. By using (14), grid frequency and active power reference under a load step event are shown in Fig. 11. Fig. 11a shows that the eIEC reduces the RoCoF and frequency nadir. In fact, the maximum frequency deviation is reduced by 0.1 Hz, while the RoCoF value is decreased by 32% for $H_v = 5\,s$. Also, Fig. 11b shows the active power injected by the power converter. It is evident that as the communication delay increases to 50 ms, the active power injected by the grid-forming power converter becomes more oscillatory. Such oscillatory behavior is due to the movement of the closed-loop pole toward the right-hand side of the s-plane. The inertia response can also be adjusted via the virtual inertia value H_v.

Fig. 12 shows the response of the eIEC under a load event. As shown, the inertia response increases when H_v is increased. It is to note that, the inertia value also contributes to the system dynamics. That is, the higher the virtual inertia the less the stable margin. In practice, the inertia constant of the generation units within a region is usually regulated by system operators to avoid adverse interactions such as power oscillations. To ensure a stable system, it is suggested that once H_v is determined D_v should be calculated accordingly.

Though it is common to consider a perturbation of around 5% for small-signal analyses [7], [25], in reality, power systems might experience more severe events. To investigate the

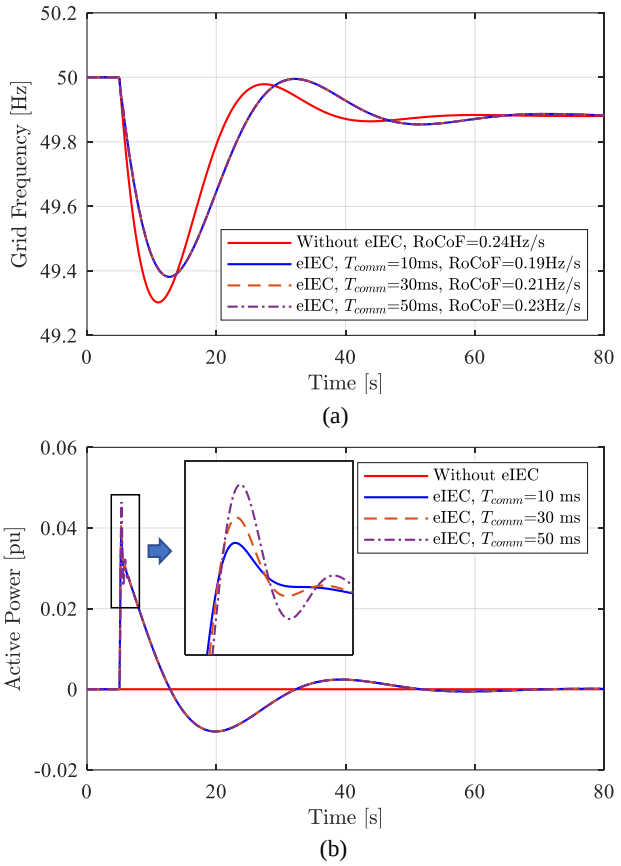

Fig. 11. System response to a load connection of 0.05 pu at 5 s for different values of communication delay: (a) Grid frequency, (b) Active power injected by the grid-following power converter.

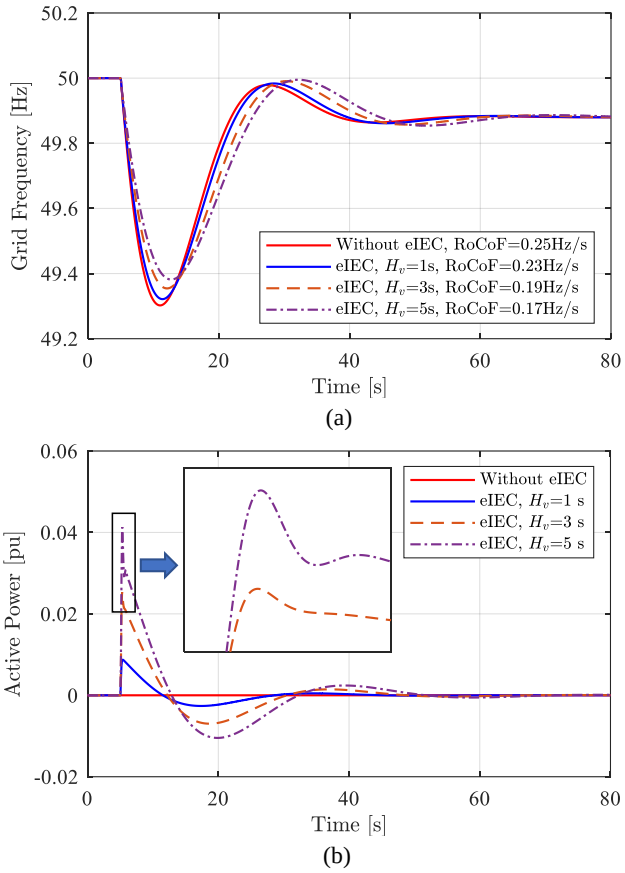

Fig. 12. System response to a load connection of 0.05 pu at 5 s for different values of communication delay: (a) Grid frequency, (b) Active power injected. by the grid-following power converter.

performance of the eIEC in the events where RoCoF values are significantly higher, simulations with a load step of 0.2 pu is considered. For such a large perturbation, the grid experiences a RoCoF value of up to 0.98 Hz/s as shown in Fig. 13. Despite the significance of the event, the eIEC can still improve the frequency response of the grid. Indeed, for all the considered delays, the eIEC is able to reduce the RoCoF value to 0.66 Hz, accounting for only 67% of the uncompensated RoCoF value. Such an improvement is consistent with that shown in Fig. 11. Evidently, the eIEC is effective even in more extreme events.

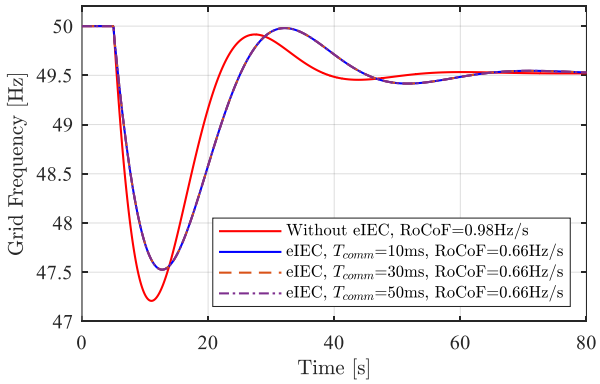

Fig. 13. Grid frequency following a load connection of 0.2 pu for different values of communication delay.

IV. Hardware-In-The-Loop Experiments

To further validate the proposed eIEC, HIL experiments have been carried out. The configuration of the experimental setup is described in Fig. 14(a) whereas the hardware setup is shown in Fig. 14(b). In this setup, the real-time simulator (Typhoon HIL 602+) is used to simulate the grid depicted in Fig. 2 and the power circuit of the power converter shown in Fig. 4. The power converter is controlled by a digital controller based on TSM320F28335 which implements the power controller, current controller, and PLL. The parameters of the power converter and its control part are shown in Table II. The proposed eIEC is designed considering that the power converter is able to comply with the grid interconnection codes and is supplied by a sufficient dc-source.

The proposed eIEC is implemented in a programable logic controller (PLC) manufactured by Beckhoff (CX9020). The communication link between the PLC and the power converter controller is based on EtherCAT Automation Protocol (EAP) which allows high communication speed e.g. up to 1 ms turnaround time. Employing such a high-speed communication link allows for emulating various settings for communication delay. For instance, Fig. 15 shows experimental measurements of communication delays for an EtherCAT Automation Protocol (EAP) link with different settings of PLC scan cycles. For the HIL experiments, turnaround times of 10, 30, 50, and 90 *ms* are considered to emulate the delay caused by the common Fieldbus protocols. Without loss of generality, a

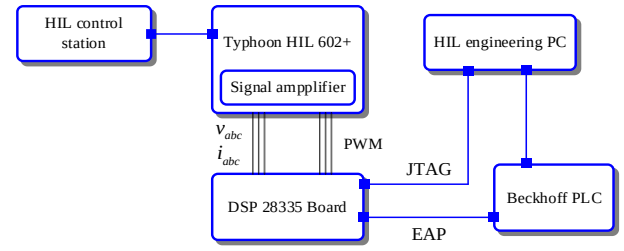

(a)

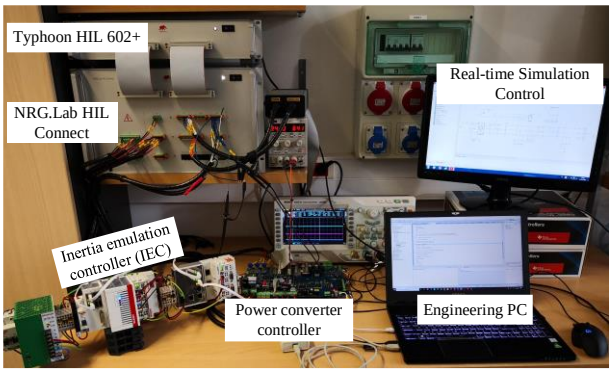

(b)

Fig. 14. Hardware-in-the-loop experimental testbed: (a) configuration. (b) hardware setup.

TABLE II
PARAMETERS OF POWER CONVERTER

Symbol	Quantity	Values
P_n	Nominal power	100 kW
V_n	Nominal voltage	400V
f_g	Grid frequency	50 Hz
f_{sw}	Switching frequency	3150 Hz
f_s	Sampling frequency	6300 Hz
V_{DC}	DC bus voltage	750 V
L_1	Inverter-side inductance	778 µH
R_1	Inverter-side resistance	7.3 mΩ
L_2	Grid-side inductance	402 µH
R_2	Grid-side resistance	2.1 mΩ
C_f	Filter capacitance	0.66 µF
R_d	Damping resistance	0.5 Ω
SCR	Short circuit ratio (SCR)	10
q	X_g/R_g ratio	7
R_g	Equivalent grid resistance	22.6 mΩ
L_g	Equivalent grid inductance	504 µH

conventional synchronous reference frame phase-locked loop (SRF-PLL) is adopted [33]. The SRF-PLL is tuned at 50 Hz which gives rise to a settling time of around 20 ms. To validate the performance of the proposed eIEC, for all experiments, a load connection event of 0.05 pu is introduced at the 5th second. Note that the 0th-second in the horizontal axis of the following HIL results indicates the starting time of data acquisition rather than the starting instance of experiments.

By using the experimental testbed, simulations conducted in the previous section are validated. Fig. 16 shows the HIL results of the eIEC with different values of communication delay. It is shown that due to the switching noise of the power converter, the injected power is distorted with high-frequency harmonics. Such harmonics are expected in power converters. Yet, the harmonics distortion does not noticeably affect the performance

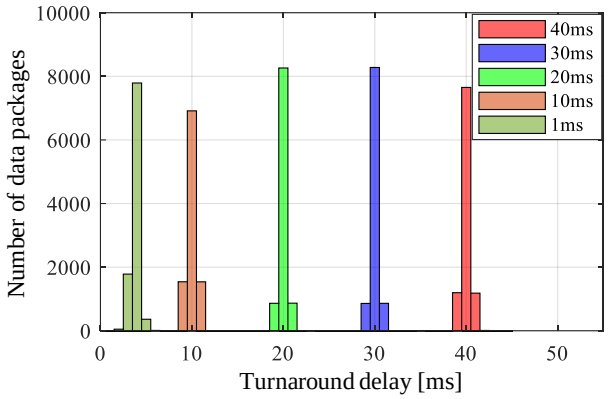

Fig. 15. Communication turnaround time for different setting of EAP.

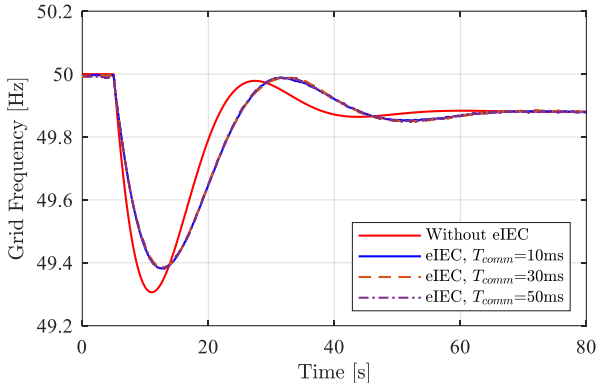

(a)

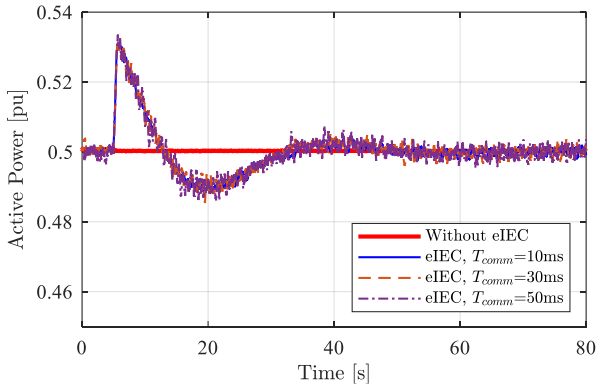

(b)

Fig. 16. HIL results for different values of communication delay. (a) Grid frequency, (b) Active power injected by the grid-following power converter.

of the proposed eIEC. That is, the difference of maximum deviation of the grid frequency and the injected active power is very small with the ones shown in Fig. 11. Similarly, Fig. 17 shows the HIL results of the eIEC for different values of virtual inertia. This proves experimentally that the active power injected by the eIEC to support the grid can be adjusted by the H_v. As clearly shown, for $H_v = 1\,s$, $H_v = 3\,s$, and $H_v = 5\,s$, the peaks of the injected active power are 0.01, 0.02, and 0.03 pu, respectively.

As analyzed in the previous section, the system stability and performance are highly linked to the communication delay, especially when the delay is substantial. As shown in Fig. 18,

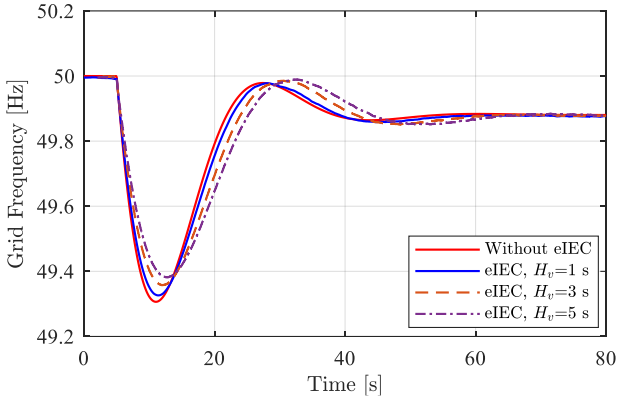

(a)

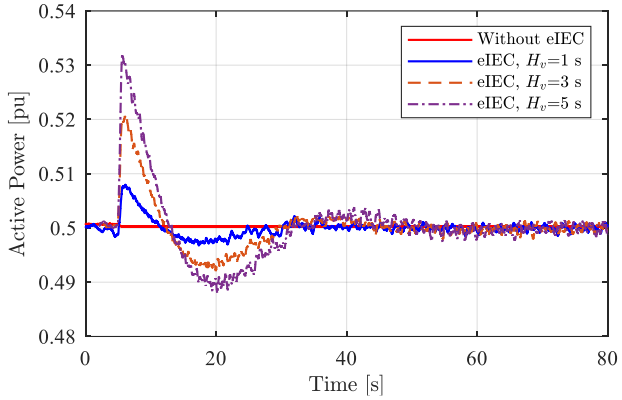

(b)

Fig. 17. HIL results for different values of virtual inertia. (a) Grid frequency, (b) Active power injected by the grid-following power converter.

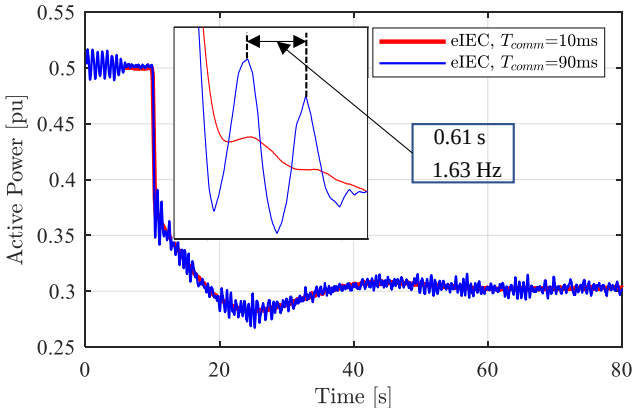

Fig. 18. HIL results for maximum allowable communication delay.

the oscillation of the injected active power decays quickly when the communication delay is 10 ms. However, once the communication turnaround increases to 90 ms, the oscillatory poles move relatively close to the imaginary axis, as shown in Fig. 10 resulting in a poorly damped response of the injected active power. Note that the oscillation frequency observed in Fig. 18 perfectly match with that of the pole depicted in Fig. 10. Concretely, the HIL results confirm the practicality of the eIEC. Moreover, these results also indicate the validity of the theoretical analyses drawn in the previous sections.

V. Conclusion

This paper presents an external inertia emulation controller (eIEC) to provide frequency support for converter dominated power systems. The eIEC is developed based on the virtual synchronous machine concept where the eIEC is designed to mimic the behavior of a synchronous generator during a frequency event. The main contribution of this work is the novel implementation of the eIEC outside the internal controller of a power converter on external control hardware. Such an implementation allows the eIEC to work with any grid-following-power converter which possesses a Fieldbus communication channel. Furthermore, the external implementation also facilitates the system operator to adjust control parameters. To ensure a stable system considering the delay introduced by communication, the tuning and performance of the eIEC is also studied by using the root locus technique. Such analyses are validated through simulations and hardware-in-the-loop experiments.

References

[1] IEA, "Renewable energy market update," Paris, 2020.
[2] K. E. N. M. Erik Ørum, Mikko Kuivaniemi, Minna Laasonen, Alf Ivar Bruseth Erik Alexander Jansson, Anders Danell, "Nordic Report: Future System Inertia," 2018.
[3] Nordic TSOs, "Challenges and Opportunities for the Nordic Power System," p. 66, 2016.
[4] ENTSO-E, "Fast Frequency Reserve – Solution to the Nordic inertia challenge," no. December, pp. 1–22, 2019.
[5] B. K. Poolla, D. Groß, and F. Dörfler, "Placement and Implementation of Grid-Forming and Grid-Following Virtual Inertia and Fast Frequency Response," *IEEE Trans. Power Syst.*, vol. 34, no. 4, pp. 3035–3046, Jul. 2019.
[6] ENTSO-E, "Need for synthetic inertia (SI) for frequency regulation," 2017.
[7] J. Fang, H. Li, Y. Tang, and F. Blaabjerg, "Distributed Power System Virtual Inertia Implemented by Grid-Connected Power Converters," *IEEE Trans. Power Electron.*, vol. 33, no. 10, pp. 8488–8499, 2018.
[8] P. Palensky and M. Van Der Meijden, "A Power Hardware-in-the-Loop Based Method Converters Control," 2020.
[9] H. P. Beck and R. Hesse, "Virtual synchronous machine," in *2007 9th International Conference on Electrical Power Quality and Utilisation, EPQU*, 2007, pp. 1–6.
[10] J. Rocabert, A. Luna, F. Blaabjerg, and P. Rodríguez, "Control of Power Converters in AC Microgrids," *IEEE Trans. Power Electron.*, vol. 27, no. 11, pp. 4734–4749, Nov. 2012.
[11] S. D. Arco, "Small-Signal Modelling and Parametric Sensitivity of a Virtual Synchronous Machine," 2014.
[12] Q. Zhong and G. Weiss, "Synchronverters: Inverters That Mimic Synchronous Generators," *IEEE Trans. Ind. Electron.*, vol. 58, no. 4, pp. 1259–1267, Apr. 2011.
[13] A. Tarraso, N.-B. Lai, C. Verdugo, I. C. J., and P. Rodriguez, "Design of Controller for Virtual Synchronous Power Plant," *IEEE Trans. Ind. Appl.*, pp. 1–1, 2021.
[14] M. A. Awal and I. Husain, "Unified Virtual Oscillator Control for Grid-Forming and Grid-Following Converters," *arXiv*, vol. 6777, no. c, 2020.
[15] W. Zhang, D. Remon, and P. Rodriguez, "Frequency support characteristics of grid-interactive power converters based on the synchronous power controller," *IET Renew. Power Gener.*, vol. 11, no. 4, pp. 470–479, 2017.
[16] A. Tayyebi, D. Groß, A. Anta, F. Kupzog, and F. Dörfler, "Frequency stability of synchronous machines and grid-forming power converters," *arXiv*, vol. 8, no. 2, pp. 1004–1018, 2020.
[17] L. Callegaro, G. Konstantinou, C. A. Rojas, N. F. Avila, and J. E. Fletcher, "Testing Evidence and Analysis of Rooftop PV Inverters Response to Grid Disturbances," *IEEE J. Photovoltaics*, vol. 10, no. 6, pp. 1882–1891, Nov. 2020.
[18] T. Kerdphol, F. S. Rahman, M. Watanabe, and Y. Mitani, "Robust

Virtual Inertia Control of a Low Inertia Microgrid Considering Frequency Measurement Effects," *IEEE Access*, vol. 7, pp. 57550–57560, 2019.

[19] Xiaorong Zhu, Yi Wang, Lie Xu, Xiangyu Zhang, and Heming Li, "Virtual inertia control of DFIG-based wind turbines for dynamic grid frequency support," in *IET Conference on Renewable Power Generation (RPG 2011)*, 2011, pp. 224–224.

[20] J. Khazaei, Z. Tu, and W. Liu, "Small-Signal Modeling and Analysis of Virtual Inertia-Based PV Systems," *IEEE Trans. Energy Convers.*, vol. 35, no. 2, pp. 1129–1138, Jun. 2020.

[21] M. Abdollahi, J. I. Candela, J. Rocabert, and M. A. Elsaharty, "Active Power Limiter for Static Synchronous Generators in Renewable Applications," *IEEE J. Emerg. Sel. Top. Power Electron.*, pp. 1–1, 2020.

[22] F. Mandrile, E. Carpaneto, and R. Bojoi, "Grid-Feeding Inverter With Simplified Virtual Synchronous Compensator Providing Grid Services and Grid Support," *IEEE Trans. Ind. Appl.*, vol. 57, no. 1, pp. 559–569, Jan. 2021.

[23] N. Hatziargyriou *et al.*, "Definition and Classification of Power System Stability Revisited & Extended," *IEEE Trans. Power Syst.*, p. 1, 2020.

[24] N. B. Lai, A. Tarraso, G. N. Baltas, L. Marin, and P. Rodriguez, "Inertia Emulation in Power Converters with Communication Delays," in *2020 IEEE Energy Conversion Congress and Exposition (ECCE)*, 2020, pp. 1665–1669, doi: 10.1109/ECCE44975.2020.9235379.

[25] P. Kundur, *Power System Stability and Control*. McGraw-Hill Education, 1994.

[26] J. Fang, H. Li, Y. Tang, and F. Blaabjerg, "Distributed Power System Virtual Inertia Implemented by Grid-Connected Power Converters," *IEEE Trans. Power Electron.*, vol. 33, no. 10, pp. 8488–8499, Oct. 2018.

[27] E. Ørum *et al.*, "Future system inertia 2," *ENTSO-E*, 2018.

[28] I. E. (IEC) Commission, "IEC 61784-2:2019 Industrial communication networks - Profiles - Part 2: Additional fieldbus profiles for real-time networks based on ISO/IEC/IEEE 8802-3," 2019.

[29] B. Ciftci, S. Schiessl, J. Gross, L. Harnefors, S. Norrga, and H.-P. Nee, "Wireless Control of Modular Multilevel Converter Submodules," *IEEE Trans. Power Electron.*, pp. 1–1, 2020.

[30] SMA, "SUNNY CENTRAL UP," 2020.

[31] ABB, "ABB central inverters," 2011.

[32] ENTSO-E, "Fast Frequency Reserve – Solution to the Nordic inertia challenge," no. December, pp. 1–22, 2019.

[33] S. K. Chung, "A phase tracking system for three phase utility interface inverters," *IEEE Trans. Power Electron.*, vol. 15, no. 3, pp. 431–438, May 2000.

NGOC BAO LAI (S'17) received the B.S. degree in electrical engineering from Danang University of Science and Technology, Da Nang, Vietnam, in 2014, and the M.S. degree in electrical and information engineering at Seoul National University of Science and Technology, Seoul, Korea, in 2017. He is currently pursuing a Ph.D. degree in electric energy systems at Universitat Politècnica de Catalunya (UPC), Spain and the Luxembourg Institute of Science and Technology (LIST), Luxembourg. His research interests include power electronics, power system stability, and networked control of distributed generation systems.

ANDRES TARRASÓ received the M.Sc. degree in electrical engineering from the Technical University of Catalonia, Barcelona, Spain, in 2017. He is currently working towards a PhD degree at the Technical University of Catalonia, Barcelona. From 2017, he has been a Research Assistant with the Department of Electrical Engineering, Technical University of Catalonia, where he has been a Researcher and an Assistant Professor with the Department of Electrical Engineering. His current research interests include power electronics, photovoltaics, wind energy systems, and microgrids.

GREGORY N. BALTAS (S'17) received the B.S. degree in electrical engineering from the Technological Educational Institute of Central Greece, Chalkis, Greece, in 2015, and the M.S. degree in power engineering from the University of Sydney, Sydney, Australia. He is currently pursuing the Ph.D. degree in data science with the Universidad Loyola Andalucía. Since 2018, he has been a Research Assistant with the Loyola Institute of Science and Technology (Loyola.TECH), Universidad Loyola Andalucía. His research interests include applied artificial intelligence, power system stability, and autonomous energy systems.

LEONARDO MARIN received the B.S. degree in Industrial Engineering from Cuenca University, Cuenca, Ecuador, in 2005, and the M.S. degree in Automatic Systems and Industrial Electronics Engineering from the Polytechnic University of Catalonia (UPC), Barcelona, Spain in 2015. He is currently pursuing his Ph.D. degree in electrical engineering at Renewable Electrical Energy System Research Centre, Universitat Politècnica de Catalunya (UPC). Since 2019, he is a research assistant at Universidad Loyola Andalucía. His research interests include the dynamic and stability analyses of power systems with high penetration of renewable energies, HVDC and hybrid systems, distributed generation systems, and microgrids.

PEDRO RODRIGUEZ (F'13) received his M.Sc. and Ph.D. degrees in electrical engineering from the Technical University of Catalonia (UPC), Spain (1994 and 2004, respectively). He was a postdoc researcher at the CPES, Virginia Tech, US, at the Department of Energy Technology, Aalborg University (AAU), Denmark and at the MIT Energy Initiative (MITie), Boston, US. He was a co-supervisor of the Vestas Power Program, Denmark (2007 – 2011). He was a director of technology on Modern Power Systems at Abengoa Research (2011-2017). From 2017, he is a full professor at the Loyola University Andalucia, where he is the Head of LOYOLA.Tech, leading a research programme on Intelligent Energy Systems. He is also linked with the UPC as a parttime professor. He is in the Clarivate's list of Highly Cited Researchers in Engineering (2015-2018). He has co-authored one Wiley-IEEE book, more than 100 papers in ISI technical journals, and around 300 papers in conference proceedings. He is the holder of 16 licensed patents. He has participated in more than 50 projects with industrial partners and several EU projects. Dr. Rodriguez is an IEEE Fellow for his contributions in the control of distributed generation. He has served as an Associate Editor of the IEEE Transaction on Power Electronics, IEEE Journal on Emerging and Selected Topics on Power Electronics, IEEE Journal on Industrial Electronics and Energies. His research interests include intelligent energy systems, distributed generation, and universal energy access.